# Dyke Award paper. MR of wallerian degeneration in the feline visual system: characterization by magnetization transfer rate with histopathologic correlation.

F J Lexa, R I Grossman and A C Rosenquist



*AJNR Am J Neuroradiol* 1994, 15 (2) 201-212
http://www.ajnr.org/content/15/2/201

*Dyke Award Paper*

# MR of Wallerian Degeneration in the Feline Visual System: Characterization by Magnetization Transfer Rate with Histopathologic Correlation

Frank J. Lexa, Robert I. Grossman, and Alan C. Rosenquist

**PURPOSE:** To examine the utility of measuring magnetization transfer ratio for delineating the dynamic changes of wallerian degeneration which occur after controlled injury in a feline model in which anatomic pathways are well understood. **METHODS:** Using standard neurosurgical techniques, discrete lesions were made to ablate the visual cortex. Gradient imaging was performed serially at 1.5 T, with and without a saturation pulse to create a magnetization transfer effect. At varying intervals, the animals were killed for histologic analysis. **RESULTS:** Within the first 2 weeks there is a statistically significant increase in magnetization transfer ratio relative to the control hemisphere within the white matter connections between the lateral geniculate nucleus and the visual cortex at a time when no effects are visually detectable on spin-echo images. Between 16 and 28 days, this reverses to a decrease in magnetization transfer ratio in both the lateral geniculate nucleus itself and the adjacent superolateral white matter. More remote white matter tracts remained stable, without significant change. **CONCLUSIONS:** Magnetization transfer ratio seems to be more sensitive for early detection of degeneration than conventional spin-echo imaging. Moreover, temporal changes in magnetization transfer ratio seem to correspond well with known histologic phases of wallerian degeneration.

**Index terms:** Wallerian degeneration; Nervous system, injuries; Magnetic resonance, experimental; Magnetic resonance, technique; Brain, magnetic resonance; Animal studies

*AJNR Am J Neuroradiol* 15:201–212, Feb 1994

Wallerian degeneration is the response of a distal axonal segment to damage to the cell body and/or the proximal axon. First described almost 150 years ago (1), it is a ubiquitous, fundamental response to injury in both the central and peripheral nervous systems. Generally, wallerian degeneration has been divided into three temporal stages (2, 3). First, axonal collapse occurs with an increase in Schmidt-Lantermann incisures (4) and physical destruction of myelin. This is followed by a second stage consisting of chemical degradation and removal of myelin lipid with edema and cellular proliferation. The third and final stage is characterized by fibrosis and volume loss. In frog peripheral nerves, endoneurial changes cause a brief increase in vascular permeability, with a later permanent increase in perineural permeability and proliferation of nonneuronal elements (5).

Computed tomography of the brain has proved capable of detecting only the later stages of degeneration, with some reports noting parenchymal hypodensity, but primarily through the observation of atrophic changes along white matter tracts (6, 7). During the past decade, rapid developments in magnetic resonance (MR) imaging of the central nervous system (CNS) have created both the opportunity and the need to

Received June 24, 1992; accepted pending revision September 14; revision received January 21, 1993.

The Cornelius G. Dyke Memorial Award is given by the American Society of Neuroradiology. This work was supported by the American Society of Neuroradiology through a Basic Science Fellowship Award for 1991–1992 (to F.J.L.), and by National Institutes of Health Grants NS-29029 (to R.I.G.) and EY-02654 (to A.C.R.). Presented at the annual meeting of the American Society of Neuroradiology, St Louis, June 1992.

From the Neuroradiology Section, Department of Radiology, Hospital of the University of Pennsylvania (F.J.L., R.I.G.), and Department of Neuroscience, School of Medicine, University of Pennsylvania (A.C.R.), Philadelphia.

Address reprint requests to Frank J. Lexa, MD, Neuroradiology Section, Department of Radiology, Hospital of the University of Pennsylvania, 34th and Spruce Streets, Philadelphia, PA 19104-4283.

AJNR 15:201–212, Feb 1994 0195-6108/94/1502–0201

obtain a better understanding of the sequence of events that underlie neural degeneration. Previous reports of clinical cases in humans and of animal injury models that used conventional spin-echo MR techniques have differed in both the nature of the observed signal patterns and the dynamic temporal sequence of those changes (8–22).

The axonal pathways of the feline visual system are one of the best understood systems in the mammalian CNS. Ablation of the visual cortex creates highly reproducible changes both in the white matter pathways that interconnect the cortex with subcortical gray matter nuclei and in the nuclei themselves: the lateral geniculate and lateral posterior pulvinar complex (23). This provides an excellent model system for examining phases of wallerian degeneration.

Magnetization transfer ratio measurement is a relatively new technique in MR imaging. This has provided useful measurements for the analysis of lesions in experimental allergic encephalomyelitis and multiple sclerosis and gives abnormal measurements in patients with multiple sclerosis, even in sectors of normal-appearing white matter (24). We undertook this study in order to see whether magnetization transfer ratio measurement would prove to be a useful probe for delineating the changes of wallerian degeneration in a well-understood animal model.

## Materials and Methods

### *Surgical Preparation*

Ten cats were used for this study. National Institutes of Health and United States Department of Agriculture regulations as well as local guidelines were adhered to in all aspects of animal care. Adult cats were screened for normal neurologic status and for normal visual perimetry. A preliminary MR study was obtained in each animal to rule out preexisting structural abnormalities. All surgical procedures were performed under aseptic conditions. Anesthesia was induced with an initial intramuscular injection of ketamine HCl (15–20 mg/kg) and atropine sulfate (0.01 mg/kg). The femoral or cephalic vein was then cannulated and an initial loading dose of pentobarbital (8–10 mg/kg) was injected intravenously. After this, procaine penicillin G (200 000 U) was given intramuscularly, and the trachea was intubated. A pulse oximeter was placed on the tongue to monitor heart rate and oxygen saturation. All subsequent anesthesia was given as a 1:1 mixture of pentobarbital and sterile saline. Supplemental doses of this mixture were given during the course of the procedure if the animal's anesthetic plane seemed to be too light as evidenced by withdrawal of the limb to pinch or an increased heart or respiratory rate. Body temperature was monitored and kept between 36.5°C and 38°C. The animal's head was then prepared for sterile surgery and placed into a stereotaxic apparatus.

### *Cortical Lesion*

A midline incision was made, and the scalp and temporalis muscle were retracted. A unilateral craniotomy was performed and extended to expose the entire cortical region to be removed. The dura was then cut and reflected, and a cortical lesion was made by gentle subpial aspiration, using landmarks that were supplied by visual cortical maps (23). This large cortical lesion removed all known visual cortical areas of the lateral, posterolateral, suprasylvian and ectosylvian gyri. Upon completion of the aspiration and the achievement of hemostasis a piece of gelfoam (Upjohn, Kalamazoo, Mich) was placed over the lesion and the tissue planes reapproximated and sutured. The animal was then removed from the sterotaxic apparatus and placed in a recovery cage where it was closely monitored until fully awake.

Imaging was then performed at varying intervals. The animal was sedated for each imaging session to alleviate any potential discomfort and to minimize motion artifacts. This required a 12- to 24-hour fast before anesthesia, which consisted of 0.02 mg/kg atropine subcutaneously followed by 8.11 mg/kg ketamine and 1.14 mg/kg acepromazine, the latter two drugs delivered intramuscularly in divided doses. MR imaging was performed at 1.5 T (Signa, General Electric, Milwaukee, Wis) using a 3-inch-round receive-only surface coil. Routine sagittal 600/20/1 (repetition time [TR] /echo time [TE]/excitations) images were obtained for localization. Three-dimensional gradient acquisition in the steady state imaging was performed using 106/5–6/1 with 12° flip angle. Twenty-eight contiguous images of 1.5-mm thickness each were collected. This was repeated with a saturation pulse in order to create a magnetization transfer effect. The saturation pulse was delivered for 19 milliseconds once per TR cycle. The amplitude was approximately 10 times the magnitude of a 90° flip angle pulse and was delivered at 2000 Hz from the center frequency of water. Several of the imaging sessions incorporated additional sequences—most commonly long-TR, four-echo (2700/20,40,60,80) images in the coronal plane without an off-resonance saturation pulse.

A custom-designed head holder was built from synthetic polymer for maintaining the cat in the Horsely-Clarke neuroanatomic plane during the imaging session and to improve reproducibility between sessions (Fig 1). This is based on the design of a similar device made of stainless steel used for the surgical ablation and histologic sectioning phases of this project.

Measurement was performed on an independent console from archived studies by comparing the signal intensity of a 1-$mm^2$ region of interest in an identical location with and without the saturation pulse. This generates a cylindrical volume of interest measuring 1.5 mm in height, with a circular configuration in the plane of section with a diameter slightly greater than 1 mm (ie, $\pi r^2 = 1\ mm^2$ or diameter equal to approximately 1.13). The formula used for mag-

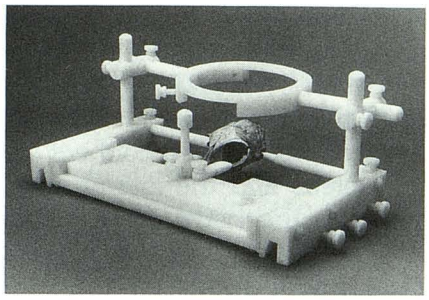

Fig. 1. Sterotaxic head holder for feline CNS MR imaging in the standard Horsley-Clark plane made from synthetic polymer.

netization transfer ratio was: (signal intensity before saturation) − (signal intensity after saturation)/Signal intensity before saturation × 100%.

Locations were chosen by consensus between a neuroradiologist and a neuroanatomist in a nonblinded fashion using a standard atlas for reference (25). The baseline or preoperative scans were sampled bilaterally at the following locations: cortical gray matter and subjacent white matter in each lobe; deep white matter: centrum semiovale, internal capsule, cerebral peduncle, and deep cerebellar white matter; deep gray matter structures: putamen, thalamus, and lateral geniculate. In addition, white matter measurements were made of the optic tract immediately before entering the lateral geniculate and in the thalamocortical white matter immediately superior and lateral to the geniculate at the origin of the optic radiations. Within a given structure, each sample site was chosen to avoid partial volume effects and to avoid overlap with other regions of interest in the same structure. Multiple samples were taken—up to seven in large structures, with a minimum of two in the smallest structures.

In the postoperative studies, the brain was again measured as symmetrically as possible from left to right in order to facilitate direct comparison of structures on the right (lesioned) side with the control left side. In addition, the sampling loci were chosen in as reproducible a manner as possible among animals and in serial examinations of the same animal. Although this process relied on visual inspection, it was facilitated by use of the head holder in conjunction with the landmarking system of the scanner. In addition, a grid technique was developed to help overcome postoperative distortion and to insure further that comparable areas were sampled on the left and right sides of the brain.

Change in magnetization transfer ratio (MTR) could then be measured for each site. This was calculated by the following formula: $\Delta MTR$ = MTR of lesioned side − MTR of control side. This gives a positive value for an increase in the amount of magnetization transfer detected on the lesioned side relative to control and a negative value for a decrease in magnetization transfer ratio. The T2-weighted coronal images were examined by two independent observers and the affected thalamocortical tracts were rated as isointense, hyperintense, or hypointense to the contralateral side.

The animals were killed at varying intervals and the brains processed for histologic examination. Four were processed for light microscopy and two for electron microscopy. The cat was given an overdose of pentobarbital (60 mg/kg intravenously) and perfused through the heart with physiological saline followed by saline containing 10% formalin (for light microscopic analysis) or a solution of 2% paraformaldehyde and 2% glutaraldehyde in phosphate buffer (for electron microscopic analysis). The brain was then postfixed and blocked in the standard stereotaxic coronal plane that corresponds exactly to the coronal plane MR images.

### *Light Microscopic Analysis*

The brain was then dehydrated through an alcohol series and embedded in celloidin. Forty-eight-micron-thick sections were cut with every 10th section Nissl stained with cresyl violet. Adjacent sections were stained for fibers by the Heidenhan-Mahon method. The extent of each cortical lesion was determined by charting the damage seen in serial coronal sections onto drawings of the hemisphere obtained from examining the intact hemisphere before sectioning. In addition, the dorsal lateral geniculate nucleus and the medially adjacent lateral posterior-pulvinar complex were examined for cellular loss and gliosis. The thalamocortical white matter, the optic radiations, and the internal capsule and cerebral peduncle were also examined and evidence for degeneration charted on drawings or photographed. No histologic data are included in this report unless the animal had undergone the complete histologic examination and reconstruction, except for the cats that are reported under electron microscopic analysis (see below).

### *Electron Microscopy*

In the two experiments using electron microscopy, tissue blocks of white matter from the white matter tracts immediately superior to the lateral geniculate were removed from the lesion and control sides of both animals. These were washed in buffer overnight followed by a 1% osmium tetroxide fixation for 1 hour, and then the overnight washing in buffer was repeated. Progressive dehydration was performed with ethanol followed by propylene oxide and then embedding in epon. Staining was performed with 40% uranyl acetate in methanol, then a methanol wash, followed by 0.3% lead citrate and finally three water washes.

## Results

Preoperative values for magnetization transfer ratio are presented in Table 1. These values represent averages from both left and right hemispheres from multiple samplings at each parenchymal locus. No significant difference from left to right was detected preoperatively in any of the animals studied. As expected, magnetization

**TABLE 1: Normal values for magnetization transfer ratio in the feline CNS**

| Locus | Magnetization Transfer Ratio (% ± SD) |
|---|---|
| Cortical gray matter | 36.13 ± 0.24 |
| Head of caudate | 36.70 ± 0.4 |
| Periacqueductal gray matter | 37.38 ± 0.25 |
| Lateral geniculate nucleus | 38.23 ± 0.17 |
| Pons | 38.63 ± 0.41 |
| Superior colliculus | 39.64 ± 0.37 |
| Thalamus | 40.41 ± 0.38 |
| Internal capsule | 41.40 ± 0.29 |
| Centrum semiovale | 41.65 ± 0.26 |
| Superolateral white matter | 41.72 ± 0.34 |
| Corpus callosum | 43.17 ± 0.31 |

Note.—Pooled data from subjects 4 and 6; total of 112 loci were sampled in symmetric pairs (left versus right).

transfer ratio was greatest in compact white matter pathways such as the corpus callosum, centrum semiovale, and internal capsule, with values from 41.4% transfer to 43.17%. Values were lower in predominately gray matter structures such as cortical gray matter (36.13%), the head of the caudate (36.7%), and periaqueductal gray matter (37.38%). Gray matter structures with significant white matter components such as the lateral geniculate nucleus, pons, superior colliculus, and thalamus had intermediate values, probably related to a contribution from myelinated tracts. Figure 2 shows the effect of a saturation pulse on contrast between gray and white matter, demonstrating the marked drop in white matter signal intensity on the saturated image that is the imaging correlate of a large magnetization transfer ratio value.

This report includes data from a total of 10 cats. Six cats were dedicated for sole use in this project and constitute the subjects in which histopathologic confirmation was obtained. Data points from an additional four cats in another experimental group are included in this report. This allowed a reduction in the anesthesia burden to the cats undergoing serial imaging. In every way, this latter group was identical to the other six: the cortical lesions were performed in an identical fashion, the imaging and data analysis were identical, and so forth. However, because the subjects in this second group were part of a protocol that required long-term survival, they were imaged less frequently in order to minimize the risk of morbidity and mortality from anesthesia. Table 2 summarizes the experimental history of all animals.

Three locations were studied for changes in magnetization transfer ratio relative to the control side. These were: 1) the white matter tracts superolateral to the geniculate nucleus, which contains reciprocal fibers that connect the lateral geniculate nucleus and the lateral posterior-pulvinar complex to the visual cortex; 2) the lateral geniculate nucleus; and 3) more remote deep white matter tracts in the centrum semiovale. (Fig 3 demonstrates regions of interest placed on

Fig. 2. Coronal gradient acquisition in the steady state images at the level of the lateral geniculate using 106/6 with 12° flip angle technique at 25 days after surgery. The *top image* is without a saturation pulse; the *bottom* has received a saturation pulse to create magnetization transfer effects. The *arrows* point out the gray-white junction with enhanced contrast after application of the pulse.

**TABLE 2: Imaging intervals and histologic analysis for all subjects of this report (10 cats)**

| Subject | Imaging Sessions (Days After Surgery) | Histologic Analysis |
|---|---|---|
| 1 | 2*, 9*, 16*, 23, 37, 44* | light microscopy, day 44 |
| 2 | 4*, 18, 25* | none |
| 3 | 1*, 9, 23, 35, 42, 49 | light microscopy, day 52 |
| 4 | 16 | light microscopy, day 16 |
| 5 | 21, 28 | light microscopy, day 29 |
| 6 | 3, 7 | electron microscopy, day 8 |
| 7 | 7, 10* | electron microscopy, day 11 |
| 8 | 7 | none |
| 9 | 16, 63 | none |
| 10 | 86 | none |

Note.—Asterisks designate studies that were analyzed for signal characteristics on spin-echo imaging.

the lateral geniculate nucleus and the superolateral white matter tracts.)

The result from a representative animal and the pooled results from all animals are plotted in Figure 4. This demonstrates an early rise in detectable magnetization transfer during the first 2 weeks with a later fall during the third and fourth weeks after lesion placement. Both the positive and negative changes are greatest in the white matter immediately superolateral to the geniculate, which is an almost pure pathway of fibers connecting the geniculate and the adjacent lateral-posterior pulvinar complex with the cortex. Statistical significance was analyzed using both a sign rank test ($P < .03$ for the rise and $P < .02$ for the fall in magnetization transfer ratio) and a $t$ test ($P < .02$ for the rise and $P < .01$ for the fall with a Bonferroni correction).

Lesser effects are seen within the geniculate itself. There is a statistically significant fall between 16 and 28 days ($P < .05$, using a $t$ test). The data suggest an early rise as well, although this did not reach statistical significance in this small group. No significant changes were seen in

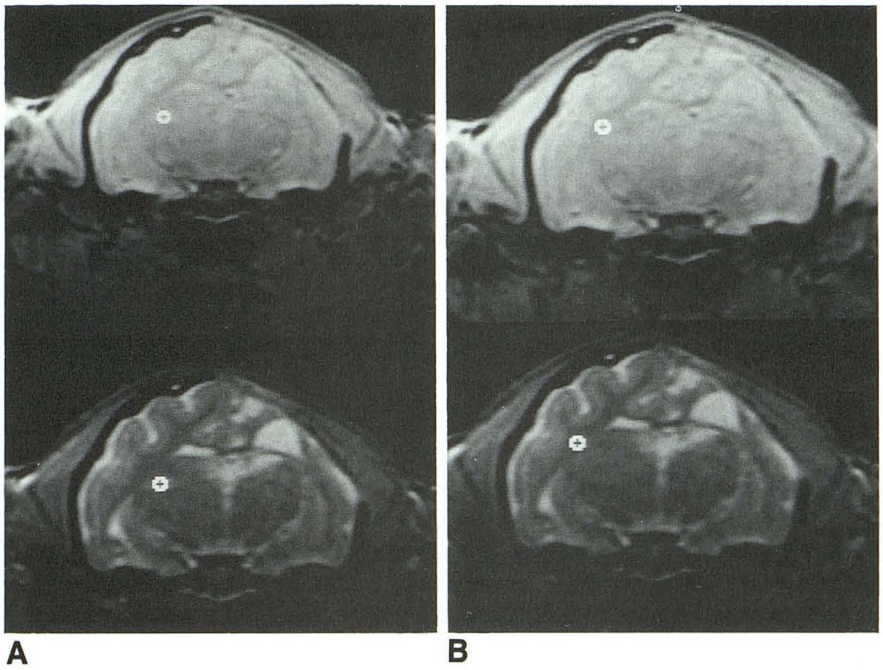


Fig. 3. Region of interest placement in an animal at 44 days after surgery. The technique is the same as for Fig 2.

*A*, Region of interest on the control side of the brain over the lateral geniculate nucleus.

*B*, Region of interest on the control side of the brain over white matter immediately superolateral to the lateral geniculate nucleus.

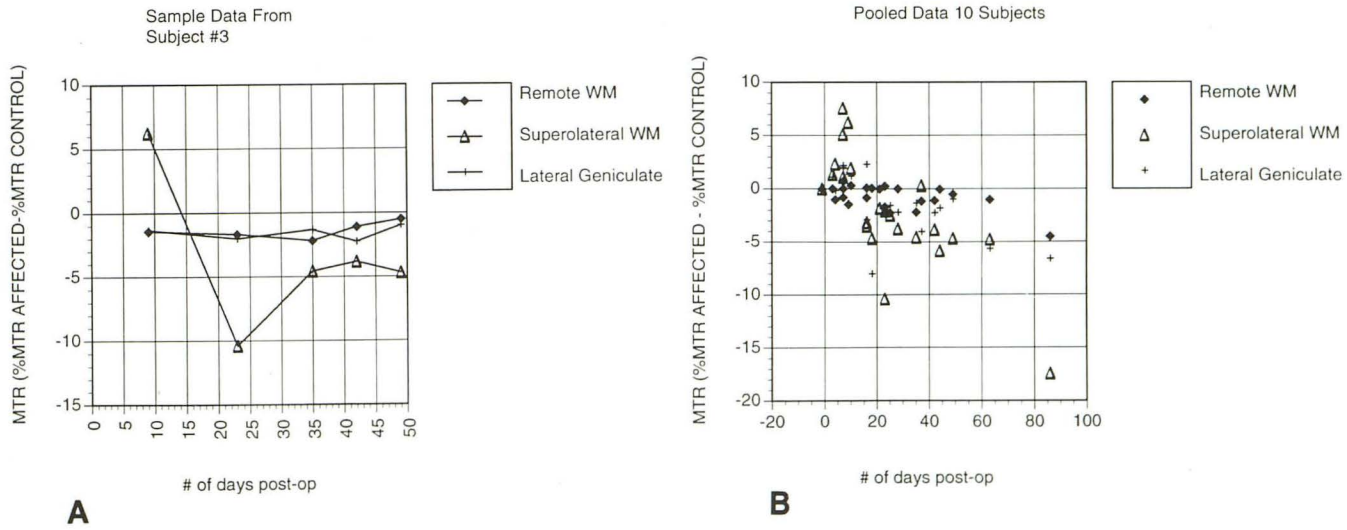


Fig. 4. Magnetization transfer ratio changes versus postoperative time.

*A*, Complete data from animal 3.

*B*, Pooled results from all animals (n = 10).

**TABLE 3: Significant effects with statistical methods applied**

| Site of Change in MTR Measurement | Days After Surgery | Change in MTR versus Control | Statistical Significance |
|---|---|---|---|
| Superolateral white matter | 0–10 | Increased | $P < .03$, sign rank test<br>$P < .02$, $t$ test |
| Superolateral white matter | 16–28 | Decreased | $P < .02$, sign rank test<br>$P < .01$, $t$ test with Bonferroni correction |
| Lateral geniculate nucleus | 16–28 | Decreased | $P < .05$, $t$ test |

Note.—This table includes data on nine of the 10 cats. The 10th was not included because it was imaged only once at 86 days and was not appropriate for the statistical methods applied. However, it also demonstrated large decreases in magnetization transfer rate (MTR) in the lateral geniculate nucleus and superolateral white matter.

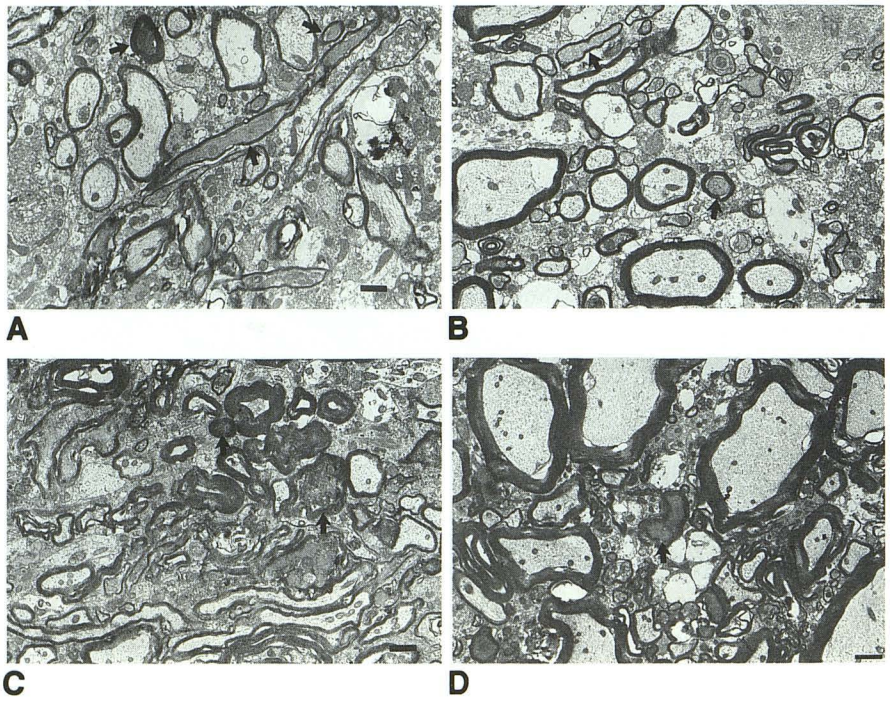


Fig. 5. *A* and *B*, Electron micrographs from white matter immediately superolateral to the lateral geniculate, ipsilateral to ablation of the visual cortex, eight days after surgery. *Arrows* demonstrate several examples of early changes of wallerian degeneration with increased axonal staining and irregularity and collapse of axons. The *black marker* represents a 1-μm calibration.

*C* and *D*, Eleven days after surgery demonstrates interval progression of changes of wallerian degeneration with more affected axons. *Arrows* mark representative examples of degenerating axons with changes as described for A and B.

more remote portions of the deep white matter. The statistical analysis is summarized in Table 3.

Although this study was performed primarily to address signal changes on magnetization transfer ratio, several of the animals also underwent long-TR/long-TE imaging when anesthesia and technical considerations allowed additional sequences. Eight studies from four separate animals were analyzed. Six of these studies showed no detectable hypointensity on proton density- and T2-weighted imaging (2700/20,40,60,80). These were performed at days 1, 2, 4, 9, 10, and 16. Two later studies performed at days 25 and 44 did show evidence for hypointensity in the thalamocortical pathways at the origin of the optic radiations relative to baseline and to the control hemisphere.

The two animals examined with electron microscopy confirmed that there were early changes of wallerian degeneration during the phase of increased magnetization transfer ratio with axonal collapse, increased axoplasmic density, and collapse of myelin tubes (Fig 5). These effects demonstrated progression from tissue processed at 8 days after surgery to the second animal killed at 11 days. In both animals, the control side showed normal axonal tracts without evidence for degeneration, inflammation, or edema (Fig 6).

Light microscopy showed chromatolytic changes in the lateral geniculate nucleus with normal-appearing adjacent white matter at 16 days (Fig 7), with neuronal loss in the geniculate and gliosis at 29 days, but again the white matter was unremarkable (Fig 8). Demyelination was seen at

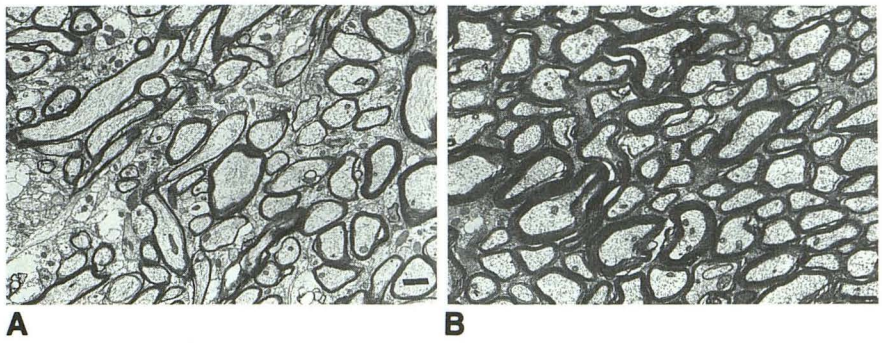


Fig. 6. Electron micrographs from white matter immediately superolateral to the lateral geniculate nucleus, contralateral to the ablated hemisphere. The *black marker* represents a 1-$\mu$m calibration.

*A*, Normal findings at 8 days after surgery; no evidence of edema, inflammation, or degenerative changes.

*B*, Normal findings at 11 days; again no evidence of wallerian degeneration.

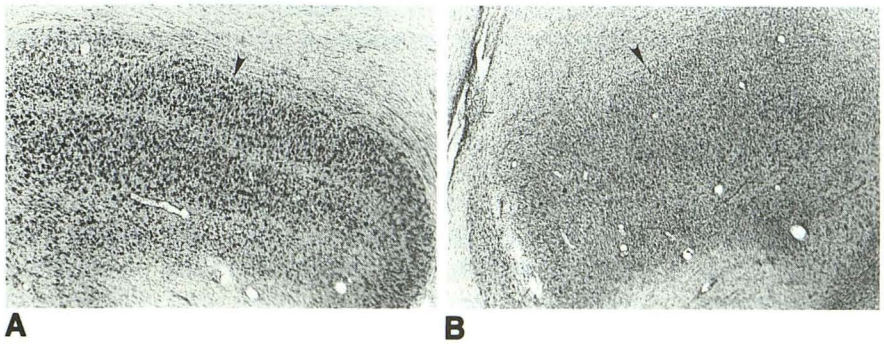


Fig. 7. Nissl stains for cellular elements of the lateral geniculate nuclei from an animal 16 days after surgery.

*A*, On the control side there is sharp definition of the margin of nucleus with adjacent white matter (*arrow*) with well-defined cellular laminae within the nucleus.

*B*, On the lesioned side there is some loss of marginal definition, and the nucleus demonstrates chromatolysis and disorganization. White matter stains (not shown) were unremarkable.

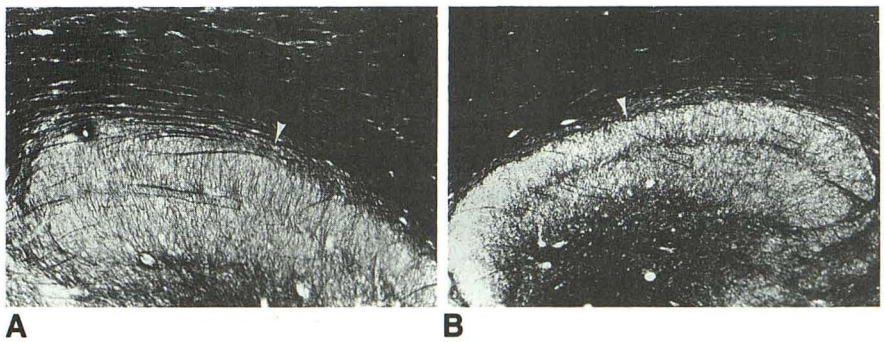


Fig. 8. Mahon stain for intact myelin (*black*) in an animal 29 days after surgery again shows no evidence for demyelination. *Arrows* point to the superior margin of the geniculate.

*A*, Control hemisphere.

*B*, Ipsilateral to ablation.

44 days with continued progression of the changes in the geniculate. By 52 days after surgery, the neuronal population in the geniculate was almost entirely depleted with gliosis in the geniculate and adjacent white matter (Fig 9A). At this time, marked demyelination was present in the superolateral white matter (Fig 9C).

## Discussion

During the nearly 150 years since Waller's original description of degeneration in peripheral nerve, the process of neuronal reaction to injury has been extensively examined (3, 26–28). Despite this detailed scrutiny, many of the histochemical events underlying wallerian degeneration remain incompletely understood, especially in the human CNS.

Investigations using MR in conjunction with an animal model are important for several reasons. First, wallerian degeneration has proved to be a powerful tool for examining pathways in the brain. Directed experiments using other species have shed important light on structural correlates in the human brain, as have natural experiments in which infarction, trauma, and other insults in humans have caused clinical syndromes that can be correlated at autopsy with structural damage. Subsequent wallerian degeneration can then be used to trace connectivity. However, there are severe limitations to this mode of inquiry. Many clinical syndromes such as the aphasias and the loss of other higher functions have no adequate animal model. Moreover, the detection of degenerating pathways in vivo would be much more illuminating, especially in examining the ability of the nervous system to compensate through secondary circuits. Optimizing the detection of degeneration and improving the understanding of its temporal phases will enhance this work.


Fig. 9. Histology from an animal at 52 days after surgery. *Arrows* mark margin of the lateral geniculate.

*A*, A Nissl stain of the control side again shows normal-appearing cellular laminae within the nucleus and a sharp border with the adjacent white matter.

*B*, A Nissl stain from the contralateral side demonstrates neuronal loss with gliosis and loss of definition with adjacent white matter, which also demonstrates gliosis.

*C*, A Mahon stain demonstrating marked loss of myelin in white matter tracts adjacent to the lateral geniculate nucleus (compare Fig 8).

Second, the past decade has seen a tremendous rise in the importance of clinical MR imaging of the human CNS. Primary and secondary demyelination in the CNS constitutes both an important source and sign of clinical disease. This has created both the need for and the opportunity to use MR technology as a probe to understand this process further.

Finally, much of the natural history of the process of demyelination and remyelination in the CNS remains only partially understood. Wallerian degeneration has played an important role in the understanding of demyelinating diseases such as multiple sclerosis. MR imaging has proved invaluable for the detection of the lesions of multiple sclerosis. Correlation of MR findings with a well-understood animal model should prove valuable for further investigations into the nature of multiple sclerosis plaques and other demyelinating processes, and evaluations of the efficacy of treatment protocols.

Work in animal models has been illuminating in correlating MR signal characteristics and underlying histochemical changes. MR spectroscopy was used (19) to examine degenerative changes in peripheral nerves and demonstrated evidence for significant prolongation of both T1 and T2 15 days after sectioning of the rat sciatic nerve. MR imaging of the rat tibial nerve (20) confirmed that prolongation of T2 occurs with hyperintense signal on long-TR/long-TE (2000/95) images at 1.9 T. This peaked at day 15 in crushed nerves and resolved at day 30. In transected nerves, maximum signal intensity was seen at day 21 and resolved by 45 to 54 days. Histopathologic examination confirmed wallerian degeneration in both the crush and neurotomy group with Schwann cell proliferation seen in the neurotomy group.

Grossman et al (21) directly examined wallerian degeneration in the CNS with MR imaging and spectroscopy in a cat model of radiation injury. Histologic confirmation was obtained. Areas of wallerian degeneration had high signal intensity on long-TR/long-TE images with gadolinium enhancement. These appeared from 208 to 285 days after radiation injury. Killing was performed from 519 to 568 days.

Rafto et al (22) examined wallerian degeneration in the CNS using a cat model with ablation of the visual cortex areas 17 to 19. For the first 12 days no abnormality was seen. They observed hypointensity on proton density- and T2-weighted images (3500/20,80) at 1.9 T, from days 13 to 48, which later normalized and became "indetectable" from 49 to 175 days. Histologic examination confirmed glial proliferation and myelin loss along the visual corticofugal fiber tract.

Differences in field strength, pulse sequences, peripheral nerve versus CNS, and interspecies variations all can be invoked to explain the above differences in qualitative and temporal findings on MR. Nevertheless, it would be useful to develop a way of detecting changes earlier and more reliably. Magnetization transfer imaging represents a relatively new application of MR imaging technology that may provide ths ability. This method was initially used by Forsen and Hoffman (29) for quantitatively measuring the rate of magnetization exchange between two chemical moieties. This is achieved by selectively saturating one

of the two exchanging species by radio frequency irradiation. Chemical exchange of saturated spins with unirradiated spins then occurs. It is well known that protein solutions demonstrate cross-relaxation phenomena occuring across the interface between proteins and solvent (30–33).

Changes in crystalline structure of proteins, which alter the availability of relaxation exchange sites, can have further significant effects on relaxation phenomena (34). Other investigations reported that measurement of cross-relaxation effects using magnetization transfer techniques provided the ability to separate protons into compartments of macromolecular bound water and free water in animal tissues and tissue-like preparations (35–38). Relaxometry techniques have shown that the structural configuration of proteins can have significant effects on proton relaxation rates (39, 40). Lipid bilayers containing cholesterol are capable of magnetization exchange with bulk water, suggesting that this may contribute to the generation of magnetization transfer ratio effect and imaging contrast in vivo (41).

These techniques have been adapted for imaging in vivo (42, 43) and seem to have the potential to generate novel forms of MR contrast. In those reports, a saturation pulse was applied off of the resonance peak of free water protons ($^1H_f$) to saturate the pool of restricted protons ($^1H_r$). These restricted protons appear as a broad band of resonances with an overall band width of approximately 20 to 40 KHz (43). Because there is rapid communication between spins within these macromolecules, "spin diffusion" (44), the saturation pulse can be applied anywhere within this range of frequencies except the relatively narrow free proton band (to avoid direct suppression of the free water peak). Communication also occurs with bound water in the surrounding hydration shell. Work using protein solutions suggests that this layer is about one water molecule thick (45). There is a boundary zone where exchange can occur between bound water and free or bulk water via either chemical exchange mechanisms or via magnetization transfer of spins. Eng et al (43) reported that through-space dipole-dipole interaction rather than chemical exchange was probably the primary mechanism based on work with hydrogen isotopes.

Cross-relaxation effects appear to have an important effect on both T1 and T2 relaxation. Wolff and Balaban (42) concluded that this pathway is particularly important in affecting observed T2 relaxation. With saturation of the restricted component, transfer effects between the free and restricted pools lead to a decrease in the signal intensity of the free component—a negative nuclear Overhauser effect. Cross-relaxation occurs with an effect on the T1 of free protons: $T_{1f} = M_o/M_s \times T_{1sat}$, Where $T_{1f}$ is the T1 of free protons in the absence of exchange, $M_o$ is the steady-state magnetization of free protons without irradiation, $M_s$ is steady state magnetization with irradiation, and $T_{1sat}$ is the observed T1 during saturation. Magnetization transfer techniques allow at least partial separation of this relaxation component, therefore potentially allowing novel forms of MR imaging contrast.

The present study demonstrates that magnetization transfer ratio measurements appear to provide information that is not readily apparent on conventional spin-echo imaging. Detectable changes are seen as early as the first week in this model of wallerian degeneration. Electron microscopy confirms definite morphologic changes of axonal shrinkage, collapse, and myelin distortion at a time when it is difficult or impossible to detect degenerative changes at the light microscopic level. Moreover, there is a clear biphasic effect with a reversal of the change in magnetization transfer ratio from positive to negative at approximately the time that changes become apparent on spin-echo imaging. Although this latter decrease is understandable by current models of magnetization transfer contrast generation, such as edema fluid or myelin changes, the early rise is more interesting but less readily explainable. We speculate that collapse of the axonal membrane into ellipsoid bodies may increase the availability of exchange sites. Other possibilities include physiochemical changes in the myelin lipid bilayer that alter the availability of cholesterol for relaxation exchange. Both this study and previous work in a similar model system (22) show no evidence for detectable changes on long-TR/long-TE images during this early period of increased magnetization transfer ratio. A later period of hypointensity was observed toward the end of the first month of degeneration and in the second month when the magnetization transfer ratio values have fallen relative to baseline. This correlates with the phase of hypointensity reported by Rafto et al (22). These observations support the premise that magnetization tranfer imaging contrast is at least partially independent of the phenomena underlying conventional spin-echo contrast.

Magnetization transfer ratio measurements seem to be able to detect affected tissue earlier than spin-echo MR, either in our own study or in published reports in humans and animal models. Histologic and chemical data clearly show changes along the axon as early as 1 or 2 days in degenerating tracts, but in previous reports MR has been unable to show changes before 2 weeks. Moreover, previous reports have varied in the number of phases of signal change that can be appreciated. In this study, at least two phases could be appreciated. In the earliest phase, a rise in magnetization transfer ratio was seen during the first 2 weeks. Later, this returned to normal and continued to drop to below baseline.

The normal CNS myelin sheath is produced by oligodendrocytes, with each oligodendroglial cell responsible for a family of CNS axons (28). Work by Fralix et al (41) and Koenig (46) using in vitro models of lipid bilayers supports the role of membrane-bound cholesterol in creating magnetization transfer effects. We speculate that physical degradation of myelin with opening of Schmidt-Lanterman clefts early in wallerian degradation may cause an increase in the available sites for magnetization transfer. This may be a contributing factor to the rise of magnetization transfer ratio seen with early changes of wallerian degeneration. Other potential causes would include increases in axonal protein content or vesicle concentration from interruption of axoplasmic transport.

Edema is probably not the primary cause for the initial rise in magnetization transfer ratio. Animals examined in the immediate postoperative period had white matter areas that appeared edematous on long-TR/long-TE imaging, but these same areas did not demonstrate a significant increase in magnetization transfer ratio relative to adjacent nonedematous white matter tracts.

A potential criticism of this work is the possibility of admixture of both antegrade and retrograde degeneration in the same model system. The geniculate and the visual cortex are interconnected. However, in these pathways, corticothalamic fibers outnumber thalamocortical fibers by about 4 million to 400 000 or a factor of 10 to 1 (47). Therefore, our model should provide an overwhelming preponderance of effects from classical wallerian degeneration. Nevertheless, this remains an important question which is best answered using systems with unidirectional fiber pathways.

Magnetization transfer ratio may prove to be a sensitive probe of the earliest changes of wallerian degeneration at a time when white matter appears normal on T2-weighted images. Further advances in detection of degenerative changes in the CNS are critical to improving sensitivity and specificity in clinical diagnosis. In addition, detection of wallerian degeneration may have important prognostic significance in the setting of stroke (48). Work on human subjects with multiple sclerosis has demonstrated that magnetization transfer ratio is capable of detecting changes in otherwise normal-appearing white matter (24). Thus magnetization transfer ratio may prove to be a useful adjunct for improving the sensitivity of MR imaging. In addition, although magnetization transfer ratio effects clearly contribute to the formation of T2 contrast in conventional spin-echo imaging, isolating magnetization transfer ratio contrast effects should create novel forms of contrast on MR imaging, which may allow the separation of wallerian degeneration from edema and other secondary effects with resultant important prognostic implications in both the central and peripheral nervous systems.

## Conclusions

There is an early reproducible rise in magnetization transfer ratio, preceding detectable changes on spin-echo imaging, which occurs during the first phase of wallerian degeneration. The presence of degenerative changes at this time was confirmed by electron microscopy.

Magnetization transfer ratio measurements comparing degenerating white matter tracts to normal white matter demonstrate a later fall in measureable magnetization transfer ratio, which correlates with the onset of the second stage of wallerian degeneration and appears to continue during the third stage.

Effects are greatest in the white matter pathways connecting the visual cortex with the lateral geniculate and the adjacent lateral/posterior pulvinar complex with both an early rise and then a later fall. The lateral geniculate shows a definite decrease in magnetization transfer ratio during the later phase with a suggestion from these data that there also may be an early rise at this site. More remote fiber pathways that would not be expected to undergo degeneration from this type of lesion did not show detectable differences in magnetization transfer ratio.

## Acknowledgments

We thank Peter Sterling, PhD, for providing expertise in the interpretation of electron micrographs, and Marcia Polansky, ScD, for her expertise in the field of statistics. We are indebted to Wendy Algeo, CLAT, for her expert care of the animals and for developing and adapting techniques of animal anesthesia for use during MR imaging, and to Norman Butler, RT, for his tireless efforts in the imaging sessions.

## References

1. Waller AV. Experiments on the section of the glossopharyngeal and hypoglossal nerves of the frog, and observations of the alterations produced therby in the structure of the primitive fibres. *Philos Trans R Soc Lond* 1850;140:423–429
2. Rossiter RJ. The chemistry of wallerian degeneration. In: Folch-Pi J, ed. *Chemical pathology of the nervous system.* New York: Pergamon Press, 1961:207–227
3. Daniel PM, Strich SJ. Histological observations on wallerian degeneration in the spinal cord of the baboon, *Papio papio. Acta Neuropathol (Berl)* 1969;12:314–328
4. Webster H, De F. The relationship between Schmidt-Lanterman insicures and myelin segmentation during wallerian degeneration. *Ann NY Acad Sci* 1964;122:29–41
5. Latker CH, Wadhwani KC, Balbo A, Rapoport SI. Blood-nerve barrier in the frog during wallerian degeneration: are axons necessary for maintenance of barrier function? *J Comp Neurol* 1991;309:650–664
6. Stovring J, Fernando LT. Wallerian degeneration of the corticospinal tract region of the brainstem: demonstration by computed tomography. *Radiology* 1983;149:717–720
7. Bouchareb M, Moulin T, Cattin F, et al. Wallerian degeneration of the descending tracts. *J Neuroradiol* 1988;1988:238–252
8. DeWitt LD, Kistler JP, Miller DC, Richardson EP Jr, Buonanno FS. NMR-neuropathologic correlation in stroke. *Stroke* 1987;18:342–351
9. Cobb SR, Mehringer CM. Wallerian degeneration in a patient with Schilder disease: MR imaging demonstration. *Radiology* 1987;162:521–522
10. Kuhn MJ, Johnson KA, Davis KR. Wallerian degeneration: evaluation with MR imaging. *Radiology* 1988;168:199–202
11. Uchino A, Onomura K, Ohno M. Wallerian degeneration of the corticospinal tract in the brain stem: MR imaging. *Radiat Med* 1989;7:74–78
12. Kuhn MJ, Mikulis DJ, Ayoub DM, Kosofsky BE, Davis KR, Taveras JM. Wallerian degeneration after cerebral infarction: evaluation with sequential MR imaging. *Radiology* 1989;172:179–182
13. Uchino A, Imada H, Ohno M. MR imaging of wallerian degeneration in the human brain stem after ictus. *Neuroradiology* 1990;32:191–195
14. Pujol JE, Mari-Vilata JL, Junque C, Vendrell P, Fernandez J, Capdevila A. Wallerian degeneration of the pyramidal tract in capsular infarction studied by magnetic resonance imaging. *Stroke* 1990;21:404–409
15. Inoue Y, Matsumura Y, Fukuda T, et al. MR Imaging of wallerian degeneration in the brainstem: temporal relationships. *AJNR Am J Neuroradiol* 1990;11:897–902
16. Danek A, Bauer M, Fries W. Tracing of neuronal connections in the human brain by magnetic resonance imaging in vivo. *Eur J Neurosci* 1990;2:112–115
17. Orita T, Tsurutani T, Izumihara A, Matsunaga T. Coronal MR imaging for visualization of wallerian degeneration of the pyramidal tract. *J Comput Assist Tomogr* 1991;15:802–804
18. Bontozoglou NP, Chakeres DW, Martin GF, Brogan MA, McGhee RB. Cerbellorubral degeneration after resection of cerebellar dentate nucleus neoplasms: evaluation with MR imaging. *Radiology* 1991;180:223–228
19. Jolesz FA, Polak JF, Ruenzel PW, Adams DF. Wallerian degeneration demonstrated by magnetic resonance: spectroscopic measurements on peripheral nerve. Radiology 1984;152:85–87
20. Titlebaum DS, Frazier JL, Grossman RI, et al. Wallerian degeneration and inflammation in rat peripheral nerve detected by in vivo MR imaging. *AJNR Am J Neuroradiol* 1989;10:741–746
21. Grossman RI, Hecht-Leavitt CM, Evans SM, et al. Experimental radiation injury: combined MR imaging and spectroscopy. *Radiology* 1988;169:305–309
22. Rafto SE, Wallace SE, Grossman RI, Rosenquist AC, Kundel HL. Magnetic resonance imaging: an animal model of CNS wallerian degeneration (abstr). *AJNR Am J Neuroradiol* 1988;9:1025–1026
23. Rosenquist AC. Connections of visual cortical areas in the cat. In: Peters A, Jones EG, eds. *Cerebral cortex.* Vol 3. New York: Plenum, 1985:81–117
24. Dousset V, Grossman RI, Ramer KN, et al. Experimental allergic encephalomyelitis and multiple sclerosis: lesion characterization with magnetization transfer imaging. *Radiology* 1992;182:483–491
25. Reinoso-Suárez F. *Topographischer Hirnatlas der Katze für experimental-physiologische Untersuchungen.* Darmstadt: E Merck AG, 1961
26. Duchen LW. In: Adams JH, ed. *Greenfield's neuropathology.* New York: Wiley, 1984;14–52
27. Kocsis JD, Waxman SG. Demyelination: causes and mechanisms of clinical abnormality and functional recovery. In: Koetsier JC, ed. *Handbook of clinical neurology.* Vol. 47. Amsterdam: Elsevier Science Publishers BV, 1985:29–47
28. Waxman SG. Structure and function of the myelinated fiber. In: Koetsier J, ed. *Handbook of clinical neurology.* Vol. 47. Amsterdam: Elsevier Science Publishers BV, 1985:1–28
29. Forsen S, Hoffman RA. Study of moderately rapid chemical exchange reactions by means of nuclear magnetic double resonance. *J Chem Phys* 1963;39:2892–2901
30. Hallenga K, Koenig SH. Protein rotational relaxation as studied by solvent $^{1}H$ and $^{2}H$ magnetic relaxation. *Biochemistry* 1976;15:4255–4264
31. Fung BM. Proton and deuteron relaxation of muscle water over wide ranges of resonance frequencies. *Biophys J* 1977;18:235–239
32. Koenig SH, Bryant RG, Hallenga K, Jacob GS. Magnetic cross-relaxation among protons in protein solutions. *Biochemistry* 1978;17:4348–4358
33. Shirley WM, Bryant RG. Proton-nuclear spin relaxation and molecular dynamics in the lysozyme-water system. *J Am Chem Soc* 1982;104:2910–2918
34. Beaulieu CF, Brown RD III, Clark JI, Spiller M, Koenig SH. Relaxometry of lens homogenates. II. Temperature dependence and comparison with other proteins. *Magn Reson Med* 1989;10:362–372
35. Edzes HT, Samulski ET. Cross relaxation and spin diffusion in the proton NMR of hydrated collagen. *Nature* 1977;265:521–523
36. Edzes HT, Samulski ET. The measurement of cross-relaxation effects in the proton NMR spin-lattice relaxation of water in biological systems: hydrated collagen and muscle. *J Magn Reson* 1978;31:207–229
37. Escanyé JM, Canet D, Robert J. Nuclear magnetic relaxtion studies of water in frozen biological tissues. Cross-relaxtion effects between protein and bound water protons. *J Magn Reson* 1984;58:118–131
38. Sobol WT, Cameron IG, Inch WR, Pintar MM. Modeling of proton spin relaxation in muscle tissue using nuclear magnetic resonance spin grouping and exchange analysis. *Biophys J* 1986;50:181–191

39. Beaulieu CF, Clark JI, Brown RD Jr, Spiller M, Koenig S. Relaxometry of calf lens homogenates, including cross-relaxation by crytallin NH groups. *Magn Reson Med* 1988;8:45–57
40. Koenig SH, Brown RD III. The raw and the cooked, or the importance of the motion of water for MRI revisited. *Invest Radiol* 1988;23:495–497
41. Fralix TA, Ceckler TL, Wolff SD, Simon SA, Balaban RS. Lipid bilayer and water proton magnetization transfer: effect of cholesterol. *Magn Reson Med* 1991;18:214–223
42. Wolff SD, Balaban RS. Magnetization transfer contrast (MTC) and tissue water proton relaxation in vivo. *Magn Reson Med* 1989;10:135–144
43. Eng J, Ceckler TL, Balaban RS. Quantitative 1H magnetization transfer imaging in vivo. *Magn Reson Med* 1991;17:304–314
44. Kalk A, Berendsen HJC. Proton magnetic relaxation and spin diffusion in proteins. *J Magn Reson* 1976;24:343–366
45. Zhong J, Gore JC, Armitage IM. Relative contributions of chemical exchange and other relaxation mechanisms in protein solutions and tissues. *Magn Reson Med* 1989;11:295–308
46. Koenig SH. Cholesterol is the determinant of gray-white contrast in MRI of brain. *Magn Reson Med* 1991;20:285–291
47. Sherman SM, Koch C. The control of retinogeniculate transmission in the mammalian lateral geniculate nucleus. *Exp Brain Res* 1986;63:1–20
48. Watanabe H, Tashiro K. Brunnstrom stages and wallerian degenerations: a study using MRI. *Tohoku J Exp Med* 1992;166:471–473